Raman – and fluorescence spectral imaging of live breast cancer cells incubated with PEGylated gold nanorods

Liesbeth Hartsuiker[1], Wilma Petersen[2], Raja G. Rayavarapu[2], Aufried Lenferink[1], André A. Poot[3], Leon W. M. M. Terstappen[1], Ton G. van Leeuwen[2,4], Srirang Manohar[2], Cees Otto[1]

[1] Medical Cell BioPhysics, MIRA-Institute for Biomedical Technology and Technical Medicine, University of Twente, P.O. Box 217, 7500 AE Enschede, The Netherlands

[2] BioMedical Photonic Imaging, MIRA-Institute for Biomedical Technology and Technical Medicine, University of Twente, P.O. Box 217, 7500 AE Enschede, The Netherlands

[3] Biomaterial Science and Technology, MIRA-Institute for Biomedical Technology and Technical Medicine, University of Twente, P.O. Box 217, 7500 AE Enschede, The Netherlands

[4] Biomedical Engineering and Physics, Academic Medical Center, University of Amsterdam, Amsterdam, The Netherlands

Abstract

The optical properties of PEGylated gold nanorods (PEG-GNR) in interaction with cells have been investigated with Raman and fluorescence microspectroscopic imaging. The emission spectra were compared with those from suspensions of GNR, which can be characterized by a broad emission bandwidth of approximately 60 nm with a band maximum around 675 nm. These properties are in good agreement with observations from various other gold substrates and (nano)particles. The emission spectra from cells incubated with PEG-GNR were dominated by Raman scattering from locations where no GNR were present. Intense fluorescence spectra, in peak-amplitude comparable with the Raman scattering from cells, were observed from locations with GNR. The frequency range of the fluorescence emission spectra coincided mainly with the Raman fingerprint region from 500 cm-1 to 1800 cm-1, excited by the laser emission line at 647.1 nm. No surface enhanced Raman spectra were observed. It was furthermore observed from cluster analysis of the Raman and fluorescence hyperspectral datasets that the GNR-related integrated fluorescence emission band from an individual cell could be sub-divided in multiple bands with slightly varying band maxima. Raman difference spectra of cells with GNR minus control cells showed that the amplitude of lipid signal in PEG-GNR-incubated cells was increased. An excellent correlation occurred between the increased lipid signals and locations of the nanorods. This positive correlation between Raman signals from lipids and fluorescence signals from gold nanorods supports that gold nanorods are locally accumulating in lipid vesicles within the cells.

Introduction

Gold nanoparticles are rapidly emerging for use in biomedical applications due to their biocompatibility and their favourable optical properties, such as an enhanced absorption cross-section at optical frequencies.[1] The latter is a result of a surface plasmon resonance, which depends on the size and geometry of the nanoparticles.[1-4]

Rod-shaped gold nanoparticles are attractive as a contrast agent as they are easy to synthesize and provide a high yield of uniform-sized particles, the size of which, and hence the peak wavelength of the plasmon absorption band, can be controlled during synthesis.[5-7] The geometry of gold nanorods (GNR) gives rise to two surface plasmon bands, one along the long axis of the nanorod and one along the short axis. The plasmon along the short axis gives rise to a high-energy resonance band at approximately 520 nm, similar to that observed from spherical gold nanoparticles. The plasmon along the long axis produces a low-energy longitudinal plasmon (LP) band. The band maximum of the absorption is very sensitive to the aspect ratio (AR) of the rod. By altering the AR of the rod, the LP resonance can be tuned towards the near-infrared (NIR) spectral region.[8] In the NIR spectral region, tissue is relatively transparent and light scattering is strongly reduced with respect to the visible and ultra-violet spectral regions. Consequentially, a relatively high penetration depth of light in tissues is achieved.

Conventional biomedical imaging techniques suffer from low contrast between tissues. However, by administering gold nanorods with NIR-surface plasmon bands (SPB) specifically to the tumor site, high contrast non-invasive cancer imaging has been achieved with techniques such as photoacoustic imaging, [9, 10] optical coherence tomography,[4] and optical [11] and Raman imaging.[12] Moreover, light absorption by the particles may cause local heating, which can be sufficient to kill cells locally.[13] Therefore, the optical properties of GNR make them promising agents for diagnostic purposes and treatment of early stage carcinomas.

The most generally used method for synthesizing GNR is the silver-assisted seed-mediated protocol [7] or one of its many variants.[5, 6] Cetyl trimethylammonium bromide (CTAB) is crucial as a shape-directing component in this method.[5, 6, 14] and gold nanorod particles have therefore been subjected to surface modification with methoxy-(polyethylene glycol)-thiol (mPEG-SH) before administration to cells in biomedical applications. Such PEGylated GNR (PEG-GNR) have been shown to be non-toxic for various cell lines.[15]

Hyperspectral Raman microspectroscopy was used to investigate the interaction of PEG-GNR with cells in more detail, Raman spectroscopy enables correlations between the optical response of the different cellular organelles and molecular components [16, 17] and the nanorods in the cells.

In addition, both the field at the laser excitation wavelength and the Raman field in resonance with the local surface plasmons of gold nanoparticles may enhance the relatively weak Raman scattering, which could result in surface enhanced Raman scattering (SERS).[18, 19] Kneipp *et al.* observed a SERS effect of gold nanoparticles which had accumulated inside endosomal compartments of living epithelial and phagocytic cells

[20] under Raman excitation conditions. It will be shown here that favourable use can be made of the intrinsic fluorescence emission properties of gold nanorods.[21,22,23] The quantum yield of the gold fluorescence emission is extremely small, but is enhanced by the field associated with the surface plasmon resonance in GNR. The GNR fluorescence emission can be efficiently excited with 647.1 nm and the emission falls well within the detection limits of the Raman emission range, between 647.1 nm and 850 nm. This situation enables simultaneous detection of Raman and fluorescence spectra of both breast cancer cells and GNR.

Materials and methods

Gold nanorod synthesis and characterisation

Gold nanorods were synthesized as previously described,[5,15] using the seed-mediated method [7,24] that requires the addition of gold seed to a growth solution with shape directing surfactant CTAB.

Tetrachloroauric acid $HAuCl_4.3H_2O$ was purchased from Acros Organics (Belgium); hexadecyltrimethylammonium bromide (CTAB > 99%), sodium borohydride ($NaBH_4$ 99%), ascorbic acid (99%) and methoxy PEG-thiol (mPEG-SH; 5000 MW) from Fluka (The Netherlands). Silver nitrate ($AgNO_3$ 99.8%) was purchased from Merck (Germany).

Freshly synthesized gold nanorod dispersions were concentrated by centrifuging twice at 7500 rcf for 20 minutes which also enabled removal of the excess unbound CTAB. After the first centrifugation cycle, the NR pellet was dispersed in MilliQ water. After the second cycle, the NR pellet was dispersed in 0.5 ml of 5 mM mPEG-SH with vigorous vortexing for 20 seconds. To this dispersion, 0.5 ml of PBS (Phosphate Buffered Saline) was added followed by continuous rotation for 24 hours at room temperature. The resultant was subjected to two centrifugation steps (7500 rcf, 20 minutes) to remove excess mPEG-SH from the dispersion and the pellet was dispersed in SK-BR-3 culture medium.

At all stages of the GNR synthesis transmission spectra were acquired, using a Shimadzu PC3101 UV-Vis-NIR spectrophotometer. Retention of the plasmon peaks in the spectra is taken as evidence of colloidal stability during the processing steps.

In addition, the spectra are used for estimating number densities as (Eq. 1):

$$N = \frac{\mu_{ext}}{Q_{ext} \cdot \pi \cdot r^2}$$

(1)

Here, μ_{ext} is the extinction coefficient of the samples calculated from transmission data, using the Beer-Lambert law. Q_{ext} is the extinction efficiency of a particle calculated using the Discrete Dipole Approximation method, DDSCAT,[25,26] and r is the radius of an equivalent sphere obtained from actual size determination from SEM images. The aspect ratio of GNR particle was derived from SEM images of at least 250 particles, The procedure was the same as shown by Rayavarapu et al.[15]

Cell culture

SK-BR-3 mammary adenocarcinoma cells were maintained using RPMI 1640 medium supplemented with 1% glutamine, 10% FBS (Fetal Bovine Serum) and 1% antibiotics (penicillin/streptomycin). The cells were passaged every 3 days.

SK-BR-3 cells were seeded on calcium fluoride (CaF_2) slides (20 mm diameter, 2 mm thickness), to obtain approximately 16.000 cells/cm^2. The cells were equilibrated over night at 37°C in a humidified 5% CO_2 atmosphere. PEG-GNR dispersed in SK-BR-3 culture medium were added to the cells resulting in a gold nanorod to cell ratio of approximately 1.6×10^6 : 1, and incubated overnight. The PEG-GNR LC50 was previously determined to be more than 2.4×10^6 nanorods per cell.[15] SK-BR-3 cultured in medium without PEG-GNR were used as a control.

The culture media were removed and the cells were washed three times with PBS after which fresh culture medium was supplied before Raman measurements of living cells commenced.

Confocal Raman microspectroscopy and imaging

Raman measurements were carried out on a confocal Raman microspectrometer similar to the setup previously described by Van Manen et al.[27] The 647.1 nm excitation light from a Krypton ion laser light source (Innova 90-K; Coherent Inc., Santa Clara, CA) was focused by a 40×/0.75 NA objective (Olympus UPFLN; Olympus, Hamburg, Germany) to measure the optical emission spectra of GNR dispersions sealed under a glass coverslip.

Raman imaging of single, living SK-BR-3 cells was performed using a 63×/1.0 NA water immersion objective (W-Plan Apochromat; Carl Zeiss, Jena, Germany). The SK-BR-3 cells were grown on CaF_2 substrate. Only SK-BR-3 cells with a spherical appearance were selected for Raman imaging. This was the preponderant cellular geometry at low seeding density. The Raman image plane was selected to be at the same height above the CaF_2 substrate in all cells. The height was adjusted based on the intensity of the 322 cm^{-1} Raman signal of CaF_2 of the substrate.

Hyperspectral Raman imaging was performed by stepping the laser beam over the sample in a raster pattern and spectral acquisition at each position with a laser power of 10mW under the objective and a dwell time of 0.5 s/pixel. The step size was 0.5 µm, which was small enough to resolve basic cell structures such as the nucleus and the cytoplasm or to detect the cell membrane.

Data analysis

All spectral data was corrected for setup response.[29] The emission spectra of GNR dispersions were averaged over 1024 (32×32) measurements to obtain a smooth average response of the non-aggregated, individual nanoparticles in the dispersion.

Univariate and multivariate analyses were performed on the hyper spectral Raman data of the SK-BR-3 cells, as described earlier.[28, 29] Noise in the resulting 3D (spatial × spatial × spectral dimension) data matrix was reduced by singular value decomposition.[28, 30] Raman images were constructed by plotting the integrated intensity of the vibrational areas of interest as a function of position. Hierarchical cluster analysis (HCA) was performed on Raman imaging data matrices to visualize regions in cells with high Raman spectral similarities. HCA is an unsupervised multivariate analysis technique that clusters spectra of high similarity together. In the cluster analysis routine, principal component analysis scores were taken as input variables, squared Euclidean distances were used as

distance measure, and Ward's algorithm was used to partition Raman spectra into clusters. All data manipulations were performed in routines written in MATLAB 7.6 (MathWorks, Natick, MA).

The reproducibility of the hyperspectral Raman data sets from individual SK-BR-3 cells was assessed by merging data sets of four cells to a 64×64 hyperspectral data set. Subsequently, multivariate analysis was performed and the results established the chemical correspondences among SK-BR-3 cells. The spectra of these control cells were compared with the spectra of SK-BR-3 cells incubated with PEG-GNR.

Cumulative Raman fingerprints of cells were obtained by summing the weighed cell clusters, after subtracting the spectrum of the cluster corresponding to the background signal, which arises due to the cell medium, following Eq. 2:

$$f = \sum_{i=1}^{j} N_p^i \cdot \left(C_i - C_{bk} \right)$$

(2)

Where N_p^i represents the number of spectra in cluster i, C_i the average cluster spectrum of cell cluster i and C_{bk} the cluster spectrum of the background.
Cumulative spectra were normalized with respect to the total Raman intensity between 150 cm^{-1} and 3600 cm^{-1}. Raman difference spectra were obtained by subtraction of normalized cumulative Raman spectra.

Results and discussion
Raman fingerprint of live SK-BR-3 cells
Figure 1A shows a white-light image of a single, live, SK-BR-3 cell with the corresponding univariate Raman intensity image in Figure 1B. The univariate image is based on the total Raman scattering in the entire fingerprint region (500-1800 cm^{-1}) and reveals the large amounts of Raman scattering from the SK-BR-3 cell. Figure 1C shows the hierarchical cluster analysis (HCA) image of the cell. Average Raman spectra calculated from each cluster can reliably be assigned to particular cellular structures.

In Figure 1C, the green cluster (Figure 1C) is recognized as the nucleus from Raman bands of DNA, the blue cluster represents the cytoplasm, which is very rich in lipids, the red cluster is assigned to the cell membrane and the black cluster is the Raman spectrum of the cell culture medium in the extra-cellular space (cluster data not shown). The cell medium spectrum has been used as a subtractant in the Raman difference spectra in Figure 1D and E.

The sum of all cell-related Raman spectra, corrected for cell medium background, is shown in Figure 1D for the fingerprint region and in Figure 1E for the high frequency region. Figures 1D and 1E show that the high scattering is predominantly due to the presence of large amounts of lipids (marked positions) in the cytoplasm of the cell (blue

cluster in Figure 1C, cluster data not shown). The high lipid content of SK-BR-3 cells is an important feature of the cells and the adenocarcinoma tissue from which the SK-BR-3 cells are derived. In general, live populations of SK-BR-3 cells exhibit low variability in the chemical composition, as was demonstrated before.[16]

Characterisation of PEGylated GNR

In Figure 2, schematic representations are shown of a gold nanorod surface before and after surface treatment. Before surface treatment, the as-prepared GNR is covered with a bilayer of CTAB, which is arranged at certain facets of the gold nanorod surface by ionic interactions [31] (Figure 2A). After treatment with mPEG-SH (5000 MW), the GNR is covered with PEG chains, which covalently bind to the gold surface (Figure 2B).

In Figure 3A, the optical extinction profiles of the GNR show the retention of the LP peak of the as-prepared GNR (solid curve, CTAB 0x), the GNR after PEGylation (dashed curve, PEG 0x) and the PEGylated GNR after washing and dispersion in cell culture medium (dotted curve, PEG 3x). The correspondence in the plasmon absorption spectra shows that the aspect ratio of the GNR is stable upon exchange of CTAB for PEG. Also, no particle clustering or aggregation has taken place. The decrease in peak intensity is due to minor losses of PEG-GNR in the washing process. The 647 nm excitation laser line for Raman is indicated with a grey line in Figure 3A, the shaded area marks the Raman detection area.

Fluorescence emission spectra of GNR with an aspect ratio of 2.5 are presented in Figure 3. Spectra have been acquired after several washing and surface treatment steps necessary for the surfactant replacement of CTAB for PEG. The solid trace (dashed trace) represents the as-prepared CTAB-GNR solution after the first (second) washing step. The dotted (dashed-dotted) profile shows the fluorescence emission spectrum of PEGylated GNR after a first (second) washing step. The fluorescence emission spectra also reflect that the surface treatment process does not change the properties of the suspensions of GNR.

In order to investigate the Raman and fluorescence emission properties of PEG-GNR in cells, the optical response of GNR was measured in a Raman spectrometer. Figure 4A shows the emission profiles of gold nanorods dispersed in MilliQ water (trace a). For comparison, the Raman response of plain MilliQ water is displayed as well (Figure 4, trace b). Both spectra clearly show the Raman OH-bending vibration around 1630 cm^{-1} and the OH-stretching vibration near 3350 cm^{-1}. The corresponding difference spectrum, presented in the inset on a nanometer scale (Figure 4A), illustrates the band shape of the broadband fluorescence response from suspended GNR. Although the aspect ratio of the GNR was 2.0 (Figure 4), the shape of the fluorescence emission spectrum is in good correspondence with GNR with aspect ratio 2.5 (Figure 3), with maxima around 660 nm and near 685 nm.

The excitation power dependence (Figure 4B; square markers) reveals a clear saturation behaviour. This is particularly pronounced in a direct comparison with the Raman signal of plain MilliQ water, which was simultaneously measured. The Raman scattering intensity of water shows the expected linear relationship with power. The saturation behaviour of the broadband features in the emission spectrum further originates from the

relatively long lifetime of the fluorescent excited state and results in the broadband emission from GNR. The emission has been attributed to sp → d interband transitions in the electronic structure of bulk gold,[21, 22, 31,32] as first reported by Mooradian in 1969.[23] The exact position of the emission maxima are related to the GNR in a shape-dependent manner and are in good agreement with previous results from the El-Sayed group.[21, 22] The GNR used for SK-BR-3 cell experiments in the remainder of this work have a longitudinal plasmon absorption maximum at 630 nm (Figure 3A), which provides then resonance conditions for the excitation and emission wavelength.

Raman fingerprint of live SK-BR-3 cells incubated with PEG-GNR
Living SK-BR-3 cells were incubated overnight with PEGylated GNR. The Raman spectrum in the fingerprint region of SK-BR-3 cells incubated with PEG-GNR changed drastically with respect to the control cultures. The bright-field image in Figure 5A shows a PEG-GNR-incubated SK-BR-3 cell with a spherical appearance, similar to the SK-BR-3 cell in Figure 1A. Spectral analysis of a 32×32 pixel map of the PEG-GNR-incubated cell shows that intense amplitudes in relatively few pixels dominate the total intensity from a SK-BR-3 cell in the univariate image in the fingerprint region (Figure 5B). These high intensity pixels are clustered together in a 7 cluster image (Figure 5C).

The corresponding cluster averages (Figure 5D, spectra a, b and c) show the presence of fluorescence emission in these clusters. It has to be noted that the blue (Figure 5D, a) and cyan cluster (Figure 5D, b) reflect spectra related to a single and double pixel event, respectively. The green spectral trace (Figure 5D, c), however, corresponds to 31 pixels and is therefore related to a more common occurrence.
As in the GNR dispersions (Figures 3B and 4A), the fluorescence emission spectrum observed in PEG-GNR-incubated SK-BR-3 cells has a large influence in the low to intermediate wavenumbers (500-1800cm^{-1}), but hardly contributes to the high frequency Raman region (Figures 5D and 5E). Due to the very high intensity of the fluorescence emission, the magenta, red and yellow cluster averages are overshadowed.

Although others have reported surface enhanced Raman scattering (SERS) from molecules at or near gold nanoparticles inside cells,[12, 20, 33, 34] we do not observe intense "SERS-like" contributions. However, normal signal levels corresponding to spontaneous Raman scattering can be observed in combination with the fluorescence emission (Figure 5D, traces a, b and c) from the PEG-GNR. In these traces, Raman peaks at 2856, 2875, 3013 and 3067 cm^{-1} are increased with respect to the cell average Raman signature (Figure 1E). This suggests colocalisation of GNR with lipid vesicles, as was previously demonstrated by others.[11, 37, 43, 44]

The GNR fluorescence from within the cells differs from that of GNR in dispersion (Figures 3B and 4A). However, as the emission profiles are particle and shape dependent,[21, 22] the varying spectral shape in Figure 5D may be a result of particle clustering within intracellular vesicles.[11, 37, 43, 44]

Figures 5F and 5G show the sum of all the spectra from the Raman images that can be attributed to the cell. The Raman spectra are corrected for medium background in the fingerprint region and the high frequency region, respectively. A comparison of the summation of the Raman spectra of the fingerprint of a whole SK-BR-3 cell incubated with PEG-GNR (Figures 5F and 5G) with that of a control and unperturbed SK-BR-3 cell reveal that both spectra are very similar. The spectral similarity suggests there is little effect of the PEG-GNR on SK-BR-3 cells.

The summation of the spectra in the fingerprint region of a PEG-GNR-incubated cell shows an increase in baseline in the first half of the wavenumber scale (Figure 5F). This is due to the fluorescence of the PEG-GNR inside the cell. However, this fluorescence contribution is not very prominent because the few pixels containing fluorescence signal are outweighed by the large number of pixels dominated by the Raman scattering of the cell. In the high wavenumber region (Figure 5G) a virtual absence of the luminescent emission renders an undisturbed view on the pronounced lipid band at 2856 cm^{-1}, which appears to be increased in terms of the unperturbed cell (Figure 1E).

Subtle changes between the incubated cells with PEG-GNR and the control cells become more apparent after spectral subtraction (Figure 6), which shows the difference spectrum of the Raman sum spectra of a PEG-GNR-incubated SK-BR-3 cell (Figures 5F and 5G) from which an unperturbed SK-BR-3 cell (Figures 1D and 1E) was subtracted.

The most prominent differences are observed in the high wavenumber Raman difference spectrum (Figure 6B), which show a shift in lipid-to-protein ratio. The Raman band at 2856 cm^{-1}, representing lipids, is increased after PEG-GNR-incubation, while protein signatures (2950-2965 cm^{-1}) are decreased. An increase in lipid expression can possibly be explained by the formation of lipid vesicles (endosomes, lysosomes), that encapsulate the PEG-GNR inside the SK-BR-3 cells.[11, 37]

Accordingly, in the fingerprint region (Figure 6A), the shift in lipid-to-protein ratio in the cell is illustrated by a decrease in the Amide bands (Amide III between 1200–1375 cm^{-1}, Amide I between 1655–1680 cm^{-1}) as well as an increase in other bands characteristic for lipids, e.g. at 1434 cm^{-1}. In addition, the fluorescence contribution of the PEG-GNR is reflected in the slope of the spectrum.

The active uptake of untargeted PEG-GNR through receptor-mediated endocytosis by cells is unlikely, because the PEG outer layer of the GNR inhibits biorecognition.[38-41] However, PEG-GNR can enter the cells by pinocytosis of extracellular fluid. As the degree of internalization of nanoparticles is directly proportional to their concentration in the medium,[42] the cells are prone to take up some PEG-GNR, which are present in excess to the cells, approximately $2.4*10^6$ nanorods per cell, albeit at a very low concentration of a few picomolar.

Inside the cell, nanoparticles cluster within endosomes or lysosomes,[11, 37, 43, 44] where molecules and particles are gathered before being secreted (exocytosis) or degraded. Since GNR fluorescence varies with the dimensions of the particles,[21, 22] GNR clustering

inside intracellular vesicles may account for the different shapes and intensities of the fluorescence response that are observed (Figure 5D). In addition, cell organelle confinement and viscosity affects the diffusion rates of GNR,[45] which vary with particle size. GNR diffusion rates influence the GNR distribution in different organelles [11] and the local fluorescence emission intensity accordingly.

The experiments reported were repeated on different individual cells. In Figure 7 the results of four individual cells were taken together and cluster analyzed as one single dataset, a so called 4-in-1 cluster analysis. The results directly illustrate the correspondence between different individual SK-BR-3 cells after PEG-GNR addition. In complete agreement with Figures 4A and 5D, the influence of the GNR fluorescence dominates in the fingerprint region (Figures 7A and 7C) and different fluorescence patterns are displayed at different locations in the cells.

In the high wavenumbers (2700-3100 cm^{-1}, Figures 7B and 7D), a region not affected by the spectral distribution of the luminescence and dominated by lipid contributions, the correspondence in intracellular chemical composition of the cells is reflected by the 4-in-1 cluster analysis. As was demonstrated before,[15] the chemical composition of live populations of SK-BR-3 is consistently measured with Raman imaging. Figure 7D shows that the increase in the Raman band at 2856 cm^{-1} is a general feature for different PEG-GNR-incubated SK-BR-3 cells. This band is characteristic for lipid molecules.

Conclusions

We have incubated SK-BR3 breast cancer cells with PEGylated gold nanorods. These PEG-GNR were acquired by PEGylation of CTAB-coated gold nanorods. The absorption and fluorescence emission spectra after each preparatory step in the conversion from CTAB-GNR to PEG-GNR showed that the aspect ratio of the gold nanorods was maintained and no evidence of aggregation was observable from the spectra. Single-cell confocal Raman microscopy with low laser doses was used to map the chemical composition of SK-BR-3 breast carcinoma cells in the presence and in the absence of untargeted PEGylated GNR after overnight incubation. The PEG-GNR nanoparticles were recognized inside the cell with the typical fluorescence emission spectrum for gold nanostructures. The plasmon enhanced fluorescence spectrum of gold nanorods, with aspect ratio's between 2.0 and 2.5, overlaps with the fingerprint region (500-1800 cm^{-1}) in the Raman spectra of SK-BR-3 cells. It was shown, by simultaneous hierarchical cluster analysis (HCA) of independently measured cells, that the optical properties of both GNR and cells, were representative for the sample.

The Raman spectra of the cells incubated in the presence and absence of PEG-GNR also revealed subtle differences. The spectral differences were related to an increase in signals at wavenumber positions common for lipid molecules. HCA of single SK-BR-3 cells and of groups of four different SK-BR-3 cells established that different cells react in a similar way to PEG-GNR incubation.

We conclude that the typical fluorescence emission of gold nanorods provides an excellent contrast to visualize the nanoparticles inside cells. The signal can be disentangled easily from the Raman signals of the cellular material itself by multivariate methods. The correlation between fluorescence emission of gold nanorods and Raman emission from cell material leads us to conclude that GNR-incubated cells have a higher lipid content then cells without GNR.

Acknowledgement

References

1.	M. A. El-Sayed, Accounts Chem. Res., **34**, 257-264 (2001).
2.	G. C. Papavassiliou, Prog. Solid State Ch., **12**, 185-271 (1979).
3.	M. Hu, J. Y. Chen, Z. Y. Li, L. Au, G. V. Hartland, X. D. Li, M. Marquez and Y. N. Xia, Chem. Soc. Rev., **35**, 1084-1094 (2006).
4.	S. J. Oldenburg, R. D. Averitt, S. L. Westcott and N. J. Halas, Chem. Phys. Lett., **288**, 243-247 (1998).
5.	G. J. Rayavarapu, W. Petersen, C. Ungureanu, J. N. Post, T. G. v. Leeuwen and S. Manohar, Int. J. Biomedical Imaging, **2007**, 1-10 (2007).
6.	R. G. Rayavarapu, C. Ungureanu, P. Krystek, T. G. van Leeuwen and S. Manohar, Langmuir, **26**, 5050-5055 (2010).
7.	B. Nikoobakht and M. A. El-Sayed, Chem. Mater., **15**, 1957-1962 (2003).
8.	S. Eustis and M. A. El-Sayed, Chem. Soc. Rev., **35**, 209-217 (2006).
9.	M. Eghtedari, A. Oraevsky, J. A. Copland, N. A. Kotov, A. Conjusteau and M. Motamedi, Nano Lett., **7**, 1914-1918 (2007).
10.	Y. W. Wang, X. Y. Xie, X. D. Wang, G. Ku, K. L. Gill, D. P. O'Neal, G. Stoica and L. V. Wang, Nano Lett., **4**, 1689-1692 (2004).
11.	J. J. Chen and J. Irudayaraj, Acs Nano, **3**, 4071-4079 (2009).
12.	X. M. Qian, X. H. Peng, D. O. Ansari, Q. Yin-Goen, G. Z. Chen, D. M. Shin, L. Yang, A. N. Young, M. D. Wang and S. M. Nie, Nat. Biotechnol., **26**, 83-90 (2008).
13.	X. H. Huang, P. K. Jain, I. H. El-Sayed and M. A. El-Sayed, Nanomedicine-Uk, **2**, 681-693 (2007).
14.	N. Lewinski, V. Colvin and R. Drezek, Small, **4**, 26-49 (2008).
15.	R. G. Rayavarapu, W. Petersen, L. Hartsuiker, P. Chin, H. Janssen, F. W. B. van Leeuwen, C. Otto, S. Manohar and T. G. van Leeuwen, Nanotechnology, **21**,1-10 (2010).
16.	L. Hartsuiker, N. J. L. Zeijen, L. W. M. M. Terstappen and C. Otto, Analyst, **135**, 3220-3226 (2010).
17.	R. E. Kast, G. K. Serhatkulu, A. Cao, A. K. Pandya, H. Dai, J. S. Thakur, V. M. Naik, R. Naik, M. D. Klein, G. W. Auner and R. Rabah, Biopolymers, **89**, 235-241 (2008).
18.	K. Kneipp, H. Kneipp and J. Kneipp, Accounts Chem Res, **39**, 443-450 (2006).
19.	M. Moskovits, J. Raman Spectrosc., **36**, 485-496 (2005).
20.	J. Kneipp, H. Kneipp, M. McLaughlin, D. Brown and K. Kneipp, Nano Lett., **6**, 2225-2231 (2006).
21.	S. Eustis and M. El-Sayed, J. Phys. Chem. B, **109**, 16350-16356 (2005).
22.	M. B. Mohamed, V. Volkov, S. Link and M. A. El-Sayed, Chem. Phys. Lett., **317**, 517-523 (2000).
23.	A. Mooradian, Phys. Rev. Lett., **22**, 185-187 (1969).
24.	A. V. Alekseeva, V. A. Bogatyrev, L. A. Dykman, B. N. Khlebtsov, L. A. Trachuk, A. G. Melnikov and N. G. Khlebtsov, Appl. Optics, **44**, 6285-6295 (2005).
25.	B. T. Draine and P. J. Flatau, J. Opt. Soc. Am. A, **11**, 1491-1499 (1994).
26.	C. Ungureanu, R. G. Rayavarapu, S. Manohar and T. G. van Leeuwen, J. Appl. Phys., **105**, 1-10 (2009).
27.	H. J. van Manen, A. Lenferink and C. Otto, Anal. Chem., **80**, 9576-9582 (2008).

28.   N. Uzunbajakava, A. Lenferink, Y. Kraan, E. Volokhina, G. Vrensen, J. Greve and C. Otto, Biophys. J., **84**, 3968-3981 (2003).
29.   V.V. Pully, A. Lenferink and C. Otto, Vibrational Spectrosc., **53**, 12-18(2010).
30.   H. J. van Manen, Y. M. Kraan, D. Roos and C. Otto, J. Phys. Chem. B, **108**, 18762-18771 (2004).
31.   M. Z. Liu and P. Guyot-Sionnest, J. Phys. Chem. B, **109**, 22192-22200 (2005).
32.   A. Bouhelier, R. Bachelot, G. Lerondel, S. Kostcheev, P. Royer and G. P. Wiederrecht, Phys. Rev. Lett., **95**, 181105 (2007).
33.   G. von Maltzahn, A. Centrone, J. H. Park, R. Ramanathan, M. J. Sailor, T. A. Hatton and S. N. Bhatia, Adv. Mater., **21**, 3175-3180 (2009).
34.   J. Kneipp, H. Kneipp, A. Rajadurai, R. W. Redmond and K. Kneipp, J. Raman Spectrosc., **40**, 1-5 (2009).
35.   R. L. Birke, J. R. Lombardi and J. I. Gersten, Phys Rev Lett, **43**, 71-75 (1979).
36.   B. N. J. Persson and A. Baratoff, Phys. Rev. Lett., **68**, 3224-3227 (1992).
37.   C. G. Wang, J. Chen, T. Talavage and J. Irudayaraj, Angew. Chem. Int. Edit., **48**, 2759-2763 (2009).
38.   T. B. Huff, M. N. Hansen, Y. Zhao, J. X. Cheng and A. Wei, Langmuir, **23**, 1596-1599 (2007).
39.   Y. L. Liu, M. K. Shipton, J. Ryan, E. D. Kaufman, S. Franzen and D. L. Feldheim, Anal. Chem., **79**, 2221-2229 (2007).
40.   T. Niidome, M. Yamagata, Y. Okamoto, Y. Akiyama, H. Takahashi, T. Kawano, Y. Katayama and Y. Niidome, J Control. Release, **114**, 343-347 (2006).
41.   D. Lankveld, R. G. Rayavarapu, P. Krystek, A. Oomen, H. Verharen, T. G. v. Leeuwen, W. d. Jong and S. Manohar, Nanomedicine-Uk, **6**, 339-349 (2011).
42.   S. D. Conner and S. L. Schmid, Nature, **422**, 37-44 (2003).
43.   B. D. Chithrani, A. A. Ghazani and W. C. W. Chan, Nano Lett, 2006, **6**, 662-668.
44.   J. W. Liaw, S. W. Tsai, K. L. Chen and F. Y. Hsu, J. Nanosci. Nanotechno., **10**, 467-473 (2010).
45.   N. Yoshida, M. Kinjo and M. Tamura, Biochem. Bioph. Res. Co., **280**, 312-318 (2001).

Figure captions

Figure 1: Raman analysis of a 32×32 Raman map of an SK-BR-3 cell acquired with 10 mW under the objective and 0.5 s dwell time per pixel: A) brightfield image; B) univariate Raman plot of the fingerprint region (500-1800 cm^{-1}); C) cluster image of 4 Raman clusters: in green the cell nucleus, in blue the cytoplasm, in red the cell membrane and black the surrounding cell medium; D) the sum of all cell related Raman spectra in the fingerprint region (500-1800 cm^{-1}) and E) in the high wavenumbers (2700-3100 cm^{-1}). Raman band positions characteristic for lipids and phospholipids are marked.

Figure 2: Schematic representation of PEGylation of the gold nanorod surface: displacement of A) CTAB, arranged at certain facets of the gold nanorod surface by B) mPEG-SH which covalently binds to the gold surface.

Figure 3: A) The extinction spectra show that 24 hours of PEGylation (dashed) and dispersion in cell culture medium after washing (dotted) do not change the optical extinction properties of the gold nanorods as synthesized (line). The 3x refers to the amount of washing steps that were conducted before the sample was subjected to measurement.The vertical line indicates the 647 nm excitation laser line for Raman, the shaded area the Raman detection area; B) ensemble Raman spectra of dispersions of non-aggregated, individual GNR display fluorescence emission in the wavenumber region corresponding to 650-810 nm show that the fluorescence emission does not change upon washing and surface treatment steps, during the exchange of CTAB for PEG. All spectra are corrected for water contribution. Spectra are offset for clarity.
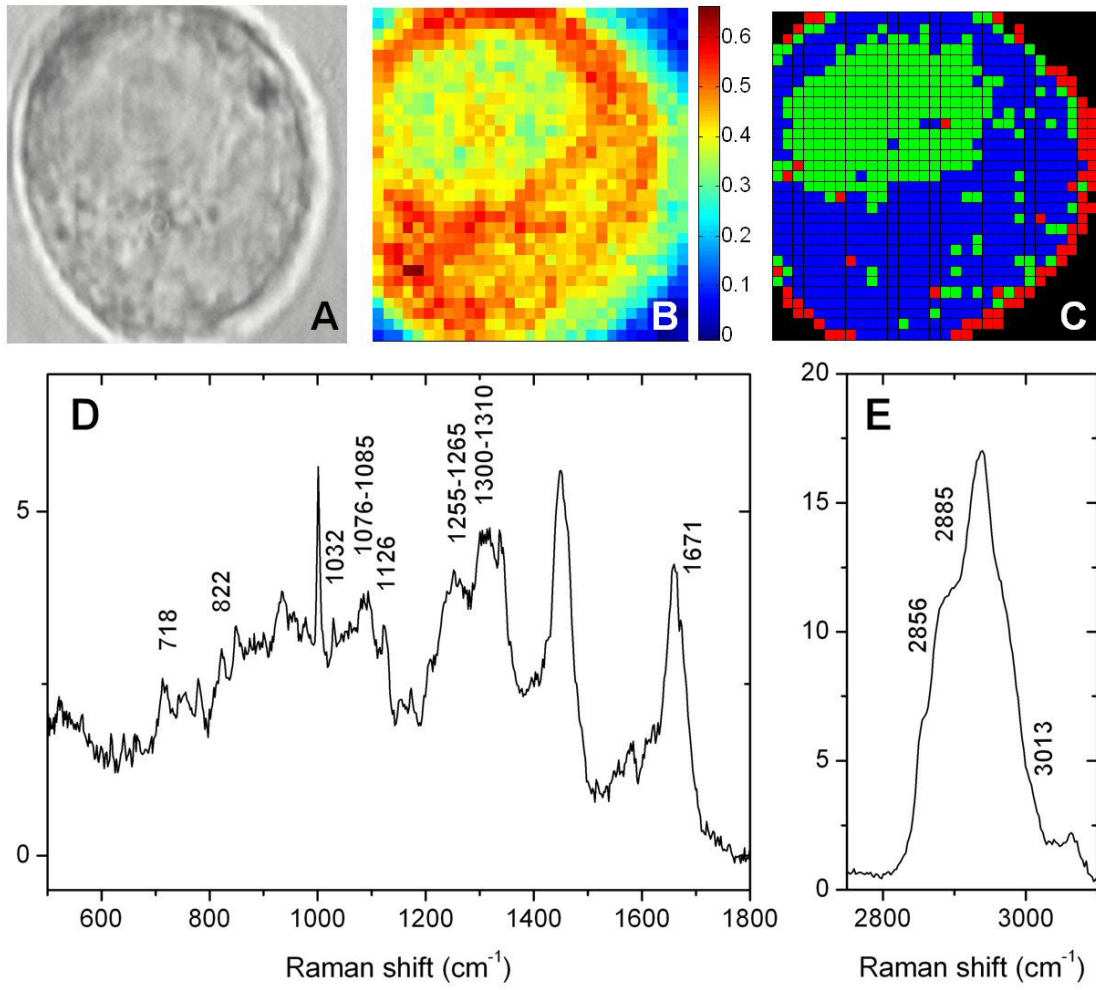
Figure 4: A) Full Raman response of a PEG-GNR solution (a) shows a broadband background contribution, whereas a regular MilliQ water solution (b) does not. Both spectra represent an average over 1024 measurements, acquired with 10mW during 0.5s. Data was corrected for setup response and normalized to the OH-stretching bands of water (3000-3600 cm^{-1}). The inset shows the corresponding difference spectrum on a nanometer scale corresponding to 75-1950 cm^{-1}. B) The broadband background contribution of the PEG-GNR solution shows a nonlinear behaviour with increasing laser power (black squares), while the OH-stretching region scale linearly with applied laser power (dots). Each data point represents an average of 200 measurements, the error bars depict the standard deviation.

Figure 5: Raman analysis of a 32×32 Raman map of an SK-BR-3 cell incubated with PEGylated gold nanorods, acquired with 10mW and 0.5s dwell time per pixel: A) brightfield image; B) univariate Raman plot of the fingerprint region (500-1800 cm^{-1}); C) cluster image of 7 Raman clusters: in red the cell nucleus, in yellow the cytoplasm, in magenta the cell membrane and black the surrounding cell medium. The green, cyan and blue pixels represent PEG-GNR fluorescence signal; D) the corresponding average cluster spectra corrected for extracellular cluster (black cluster in C) in the fingerprint region (500-1800 cm^{-1}) and E) in high wavenumber region (2700-3100 cm^{-1}) showing dominating broadband contributions (a-c); F) the weighed sum of all cell related Raman spectra shows that gold nanorod fluorescence dominates the Raman signal in the

fingerprint region while in G) the high wavenumbers the fluorescence influence is negligible. Raman bands indicating the GNR-induced shift in lipid-protein ratio are marked.

Figure 6: Difference Raman spectra of an SK-BR-3 cell before and after 24 hour of PEG-GNR incubation shows GNR fluorescence in A) the fingerprint region (500-1800 cm^{-1}) and enhanced lipid Raman signal in B) the high wavenumbers (2700-3100 cm^{-1}).

Figure 7: Four different SK-BR-3 cells incubated with PEGylated gold nanorods were subjected to a single hierarchical cluster analysis (HCA) of 4 levels showing the presence of a dominating feature in A) the fingerprint region (500-1800 cm^{-1}), while in B) the high wavenumbers (2700-3100 cm^{-1}) still the identical overall intracellular chemical composition is reflected. All cells were imaged with 10 mW under the objective and 0.5 s dwell time per pixel. Corresponding cluster averages are depicted in C) and D) respectively.
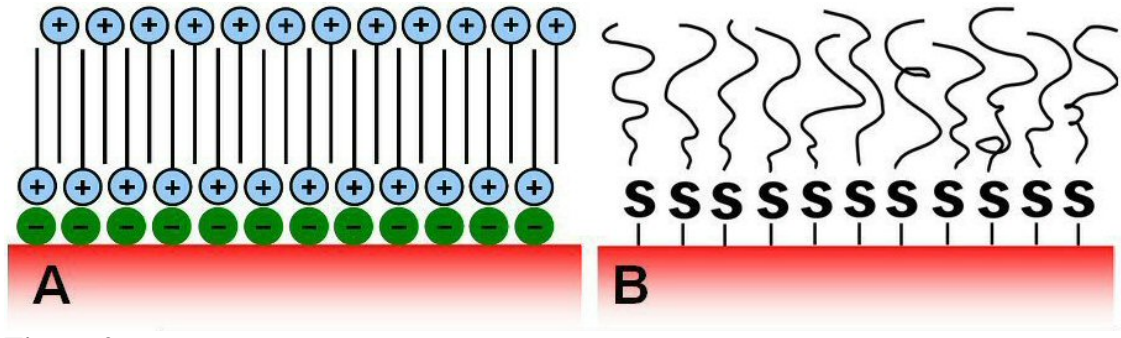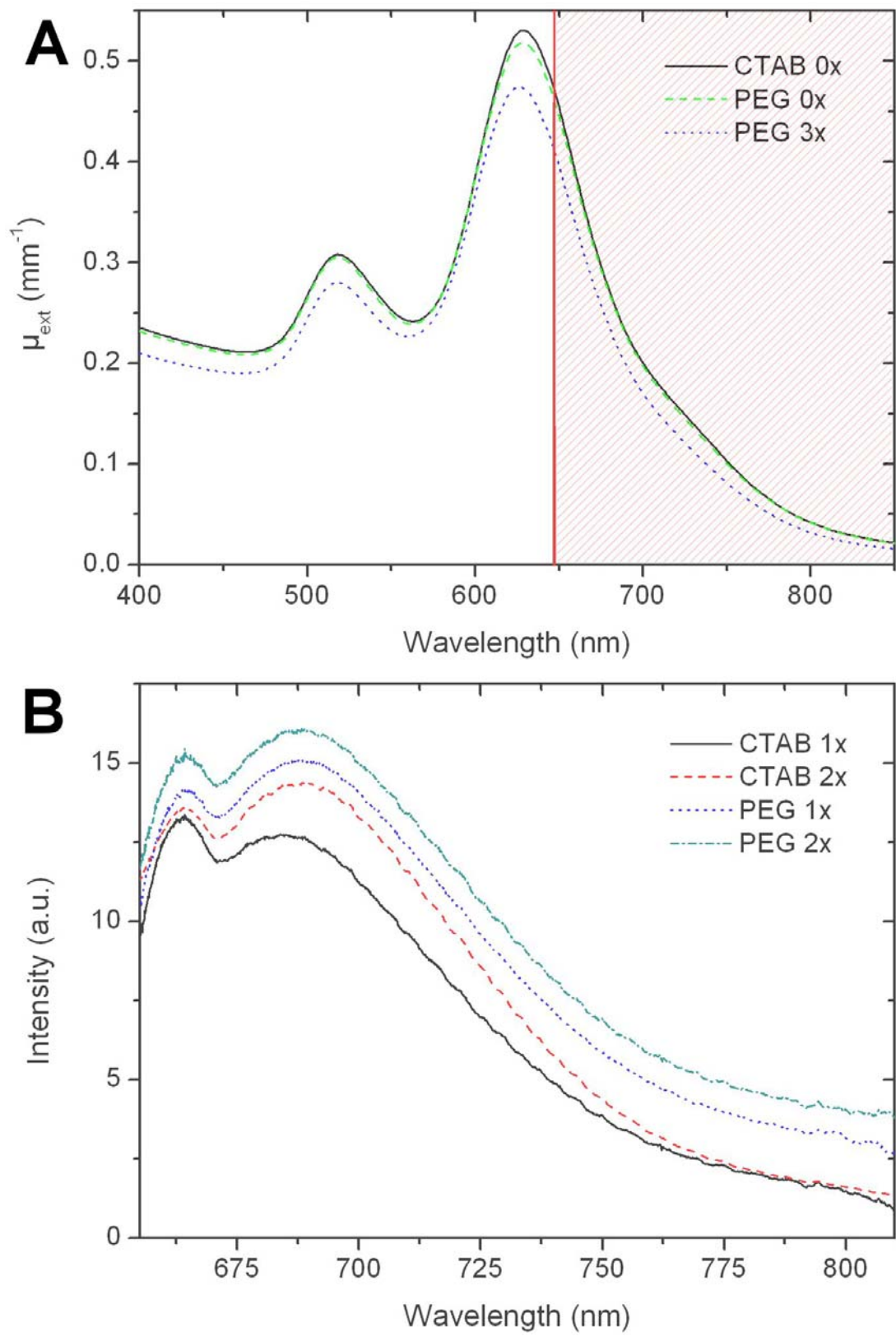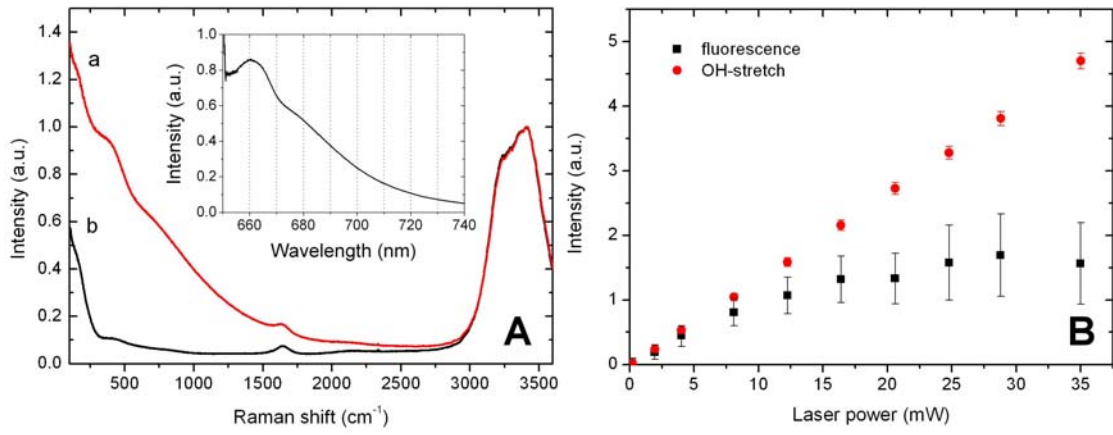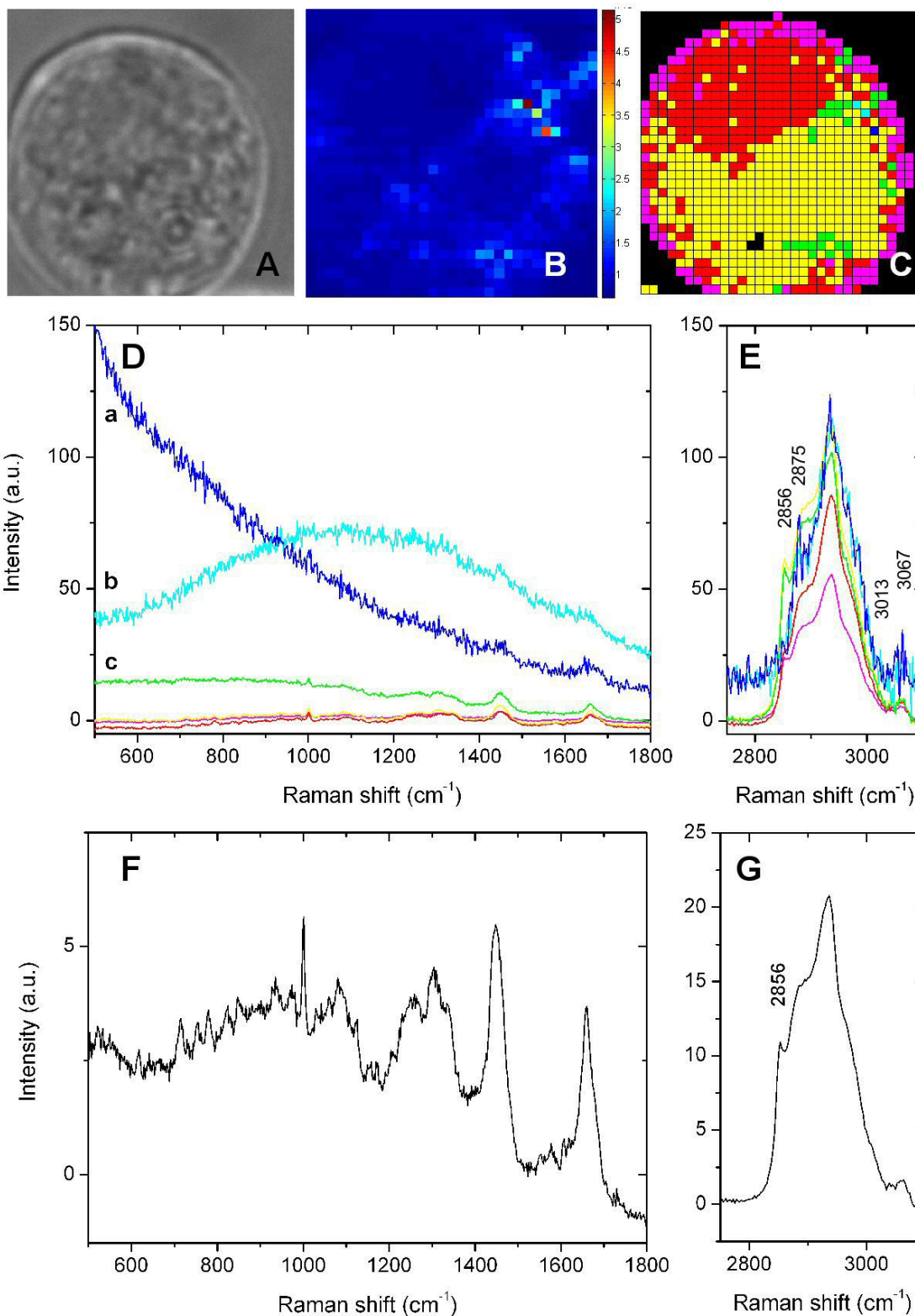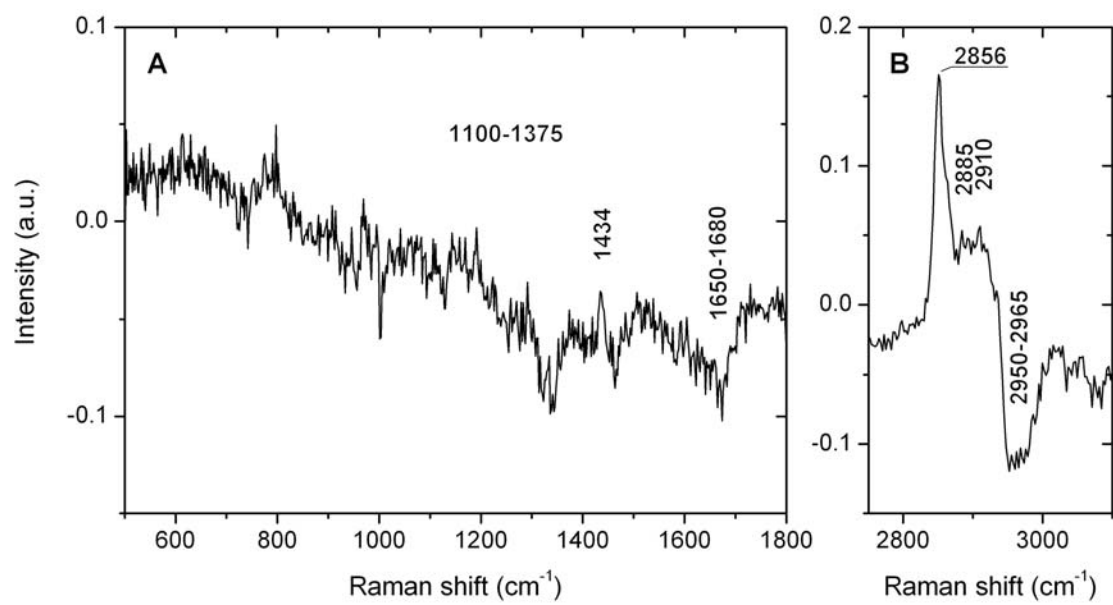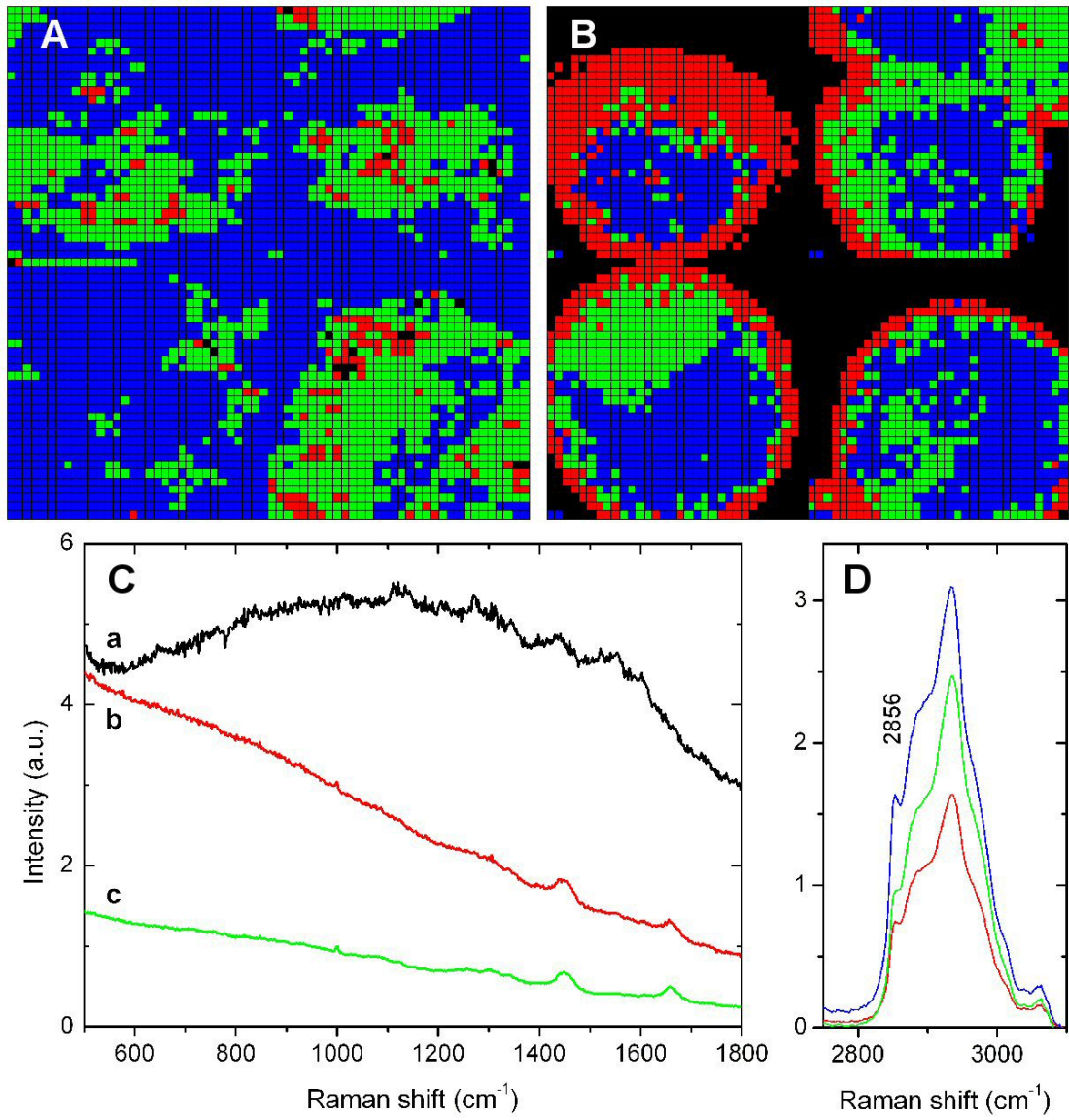
Figure 1

Figure 2

Figure 3

Figure 4

Figure 5

Figure 6

Figure 7